RSC Advances

PAPER

View Article Online
View Journal | View Issue

Cite this: *RSC Adv.*, 2025, **15**, 569

Facile development of carbon nanotube (CNT)-based flexible thermoelectric materials for energy-harvesting applications

Nimra Naeem, [a] Sajid Butt, *[a] Sumayya,[b] Zoha Afzal,[a] Muhammad Waseem Akram, [a] Muhammad Irfan, [a] Muhammad Atiq Ur Rehman,[b] Abrar H. Baluch,[cd] Ghufran ur Rehman[e] and Muhammad Umer Farooq[f]

Received 19th April 2024
Accepted 30th November 2024

DOI: 10.1039/d4ra02914c

rsc.li/rsc-advances

In this study, we investigate the thermoelectric properties of functionalized multi-walled carbon nanotubes (F-MWCNTs) dispersed over a flexible substrate through a facile vacuum filtration route. To improve their interfacial adhesion and dispersion, F-MWCNTs underwent hot-pressing. The heat-treatment has improved the nanotubes' connections and subsequently reduced porosity as well, which results in an increasing electrical conductivity upon increasing temperature of hot-pressing. Thermoelectric power factor (PF) value was greatly increased upon simultaneous heating and pressing of the CNTs and a highest PF value of 3.17 μW m^{-1} K^{-2} at 398 K, has been achieved, which is about 400% higher than that of the as-deposited CNTs without hot pressing. The current study presents a prototype for CNT-based flexible thermoelectric devices which opens up an avenue for the deployment of CNTs into flexible electronics.

1. Introduction

Lawrence Livermore National Laboratory published a report claiming about one-third of the world's primary energy is utilized effectively while the rest is wasted in the form of heat release.[1] Extensive research is being carried out on the efficient utilization of energy sources[2] and among those, thermoelectric (TE) technology is gaining immense importance due to its ability in direct conversion of waste heat into electricity. The efficiency of any TE material is assessed using a dimensionless figure-of-merit $ZT = \left(\frac{\sigma S^2}{K}\right)T$, here, σS^2 is explicitly defined as power factor (PF) while σ, S, k and T are the electrical conductivity, Seebeck coefficient, thermal conductivity and operating temperature, respectively.[3–5] To explore potential enhancements in thermoelectric (TE) performance, we must adjust the fundamental thermoelectricity parameters. Achieving a high PF corresponds to the most economical production of electricity, especially in cases where the energy source is "free", such as solar heat or recovered waste heat from automobiles and power plants.[6,7] The efficiency of available TE materials is insufficient to replace conventional electricity generators and refrigerators, in addition to that the commercially available TE devices often rely on elements that are rare or considered hazardous.

In recent years, a variety of solutions to these issues have been put up.[4,8] To attain high-performance thermoelectric materials, researchers have looked into a number of material classes, including chalcogenides,[9–11] oxides,[8,12–16] skutterudites,[17–19] half-Heuslers,[20–22] and clathrates.[23–25] Doping of them with suitable materials enhance their thermoelectric properties.[26–28] In thermoelectrics, the selection of a material depends upon several factors including upper temperature range, required efficiency, availability and cost-effectiveness. Carbon nanotubes (CNTs) have received a great deal of interest since their discovery in 1991.[29–32] They pose clear advantages, over other conventional thermoelectric materials, due to high electrical conductivity, moderate Seebeck coefficient,[33,34] low thermal conductivity,[35] low density,[36] high melting point and mechanical flexibility. They are cylindrical molecules made up of carbon atoms arranged in a hexagonal lattice offering 1D structures constructed entirely of carbon (sp^2 hybridization).[37,38] There are two types of CNTs; single-walled CNTs and multi-walled CNTs.[39] CNTs are inherently non-polar and insoluble in polar solvents like water and to improve their dispersion and compatibility with various matrices, such as polymers or composites, they need to be chemically modified

[a]*Department of Space Science, Institute of Space Technology, Islamabad 44000, Pakistan*

[b]*Department of Materials Science and Engineering, Institute of Space Technology, Islamabad 44000, Pakistan. E-mail: sajid.butt@ist.edu.pk*

[c]*Department of Aerospace Engineering, King Fahd University of Petroleum & Minerals, Dhahran, Saudi Arabia*

[d]*Interdisciplinary Research Center for Aviation and Space Exploration, King Fahd University of Petroleum & Minerals, Dhahran, Saudi Arabia*

[e]*Department of Materials Science and Engineering, Pak-Austria Fachhochschule, Institute of Applied Sciences and Technology, Haripur, Pakistan*

[f]*Department of Physics, University of Education (Lahore), Faisalabad Campus, Lahore, Punjab, Pakistan*

by attaching polar functional groups.[40,41] Dispersion of CNTs is a practical challenge due to the significant difference in surface energy between CNTs and typical organic solvents or polymers. This difference in energy can hinder proper dispersion and in order to address this issue, CNTs can be functionalized through chemical (covalent) or physical (non-covalent) methods.[42] Covalent functionalization involves breaking some C=C double bonds in the single-walled carbon nanotubes or altering the exterior wall of multi-walled carbon nanotubes. This modification affects both electrical and mechanical properties making it a common choice for TE applications after surface modifications. CNTs are often chemically modified through acid oxidation processes using agents like hydrochloric acid,[43] nitric acid[44] and a mixture of sulfuric acid and nitric acid.[45] This modification introduces oxygenated functional groups attached to the CNTs surface, addressing hydrophobicity issues and enhancing electron transfer rates as well.[46,47] These functional groups improve CNTs' solubility into aqueous environments and increase their electrical conductivity, making them more suitable for thermoelectric use. The vacuum filtering process, also known as the "Bucky paper" method, involves dispersing CNTs in a suitable solvent and breaking apart CNT bundles through sonication or other means. The resulting dispersion is then applied to a porous membrane and vacuum filtered to remove the solvent, leaving behind a CNT film. By altering the type and concentration of CNTs in the dispersion and adjusting filtration conditions, we can tailor the film's characteristics.[48–50] These CNTs films find applications in various fields, including electronic devices,[51,52] sensors,[53–55] and energy storage,[56–58] making them valuable for thermoelectric applications. Additionally, there are studies suggesting that hot pressing CNT films over flexible substrates can enhance their thermoelectric properties. For instance, Lee *et al.*[59] demonstrated improvements in the thermoelectric characteristics of CNT/conjugated polymer nanocomposite films through hot pressing. They observed that the thermoelectric power factor of the CNT/P3HT and CNT/PEDOT:PSS nanocomposite films increased significantly. Specifically, the power factor increased from 150 ± 9 to 217 ± 30 $\mu W\ m^{-1}\ K^{-2}$ for CNT/P3HT and from 371 ± 44 to 572 ± 92 $\mu W\ m^{-1}\ K^{-2}$ for CNT/PEDOT:PSS after hot pressing. Moreover, Kumanek *et al.*[60] improved their electrical conductivity up to 11.6 S cm^{-1} at 800 °C by adding 2% ferrocene catalyst. A study by Cao Liyang, *et al.*[61] reveals that the electrical conductivity of MWCNTs can be enhanced through hot press treatment. This technique involves applying heat and pressure to MWCNTs, thereby improving their electrical conductivity by strengthening the interface bonding between the MWCNTs and the surrounding matrix. This method is particularly effective for MWCNT/PVA buck papers, where hot press treatment at 70 °C significantly increased the electrical conductivity from 463.5 S m^{-1} to 714.3 S m^{-1}.

In the present work, functionalization of multi-walled carbon nanotubes (MWCNTs) through acid treatment followed by their deposition over flexible substrates using vacuum filtration technique with subsequent hot-pressing, has been adopted to improve performance of CNTs. Despite extensive research on thermoelectric materials, there are no reports on the thermoelectric properties resulting from the straightforward method of creating films on bulky filter paper followed by hot pressing. However, the literature contains numerous reports on the functionalized multi-walled carbon nanotubes (MWNTs). Some studies incorporate various nanoparticles with CNTs,[62–65] others utilize different types of acids,[66] and still, others employ different approaches for film fabrication.[67,68] Meanwhile, some investigations explore the electrical conductivity of these materials for various applications, such as optical properties. Additionally, we investigated the impact of hot pressing at different temperatures while keeping the pressure and time constant. Functionalization of CNTs involves modification of their surfaces to target TE applications.

2. Experimentation

2.1 Materials and methods

For acid treatment, a solution of 100 ml sulphuric acid (H_2SO_4) 96% and nitric acid (HNO_3) 69% concentrated were mixed in a fixed ratio of 3 : 1. 10 mg of multi-walled carbon nanotubes (MWCNTs), supplied by Guangzhou Jiechuang trading Co., Ltd China, was slowly added into the obtained acidic solution and was kept on stirring at 80 °C for 24 h. During this process, NH_3 was introduced to interact with the nanotube structure. After that, the MWCNTs are filtered using vacuum filtration with a membrane filter paper "0.22 μm pore size". To neutralize the pH of acid treated MWCNTs layer formed on the filter paper, washing with deionized water is carried out several times. After neutralization, the filter paper is removed from the vacuum filtration setup and dried in an oven. To prevent any damage or burning of the paper, we subjected it to heating at 80° for 2 hours. The film of F-MWCNTs is cut into strips of 5 mm × 13 mm. The strips of F-MWCNTs deposited over filter paper were then subjected to hot pressing at different temperatures of 80 °C, 100 °C, 120 °C and 200 °C under a uniaxial load of 1 ton for 60 s, as given in Table 1. All the experimental sequence along with necessary information is illustrated in Fig. 1.

2.2 Characterizations

The information about functionalization and surface modifications of CNTs was obtained using Fourier transform infrared spectroscopy (FTIR) manufactured by Thermo Nicolet 6700. Ramman spectroscopy (i-Raman® EX portable Raman) equipped with 1064 nm laser excitation was used to study the intramolecular and intermolecular compositions of samples. The structural quality of CNTs was determined by comparing the

Table 1 A series of all the functionalized multi-walled carbon nanotubes (F-MWCNTs) deposited over flexible substrate followed by hot-pressing at different temperatures

S. no.	Compositions	Abbreviations
1	F-MWCNTs without hot-pressing	S1-FC
2	F-MWCNTs hot-pressed at 80 °C	S2-80
3	F-MWCNTs hot-pressed at 100 °C	S3-100
4	F-MWCNTs hot-pressed at 120 °C	S4-120
5	F-MWCNTs hot-pressed at 200 °C	S5-200

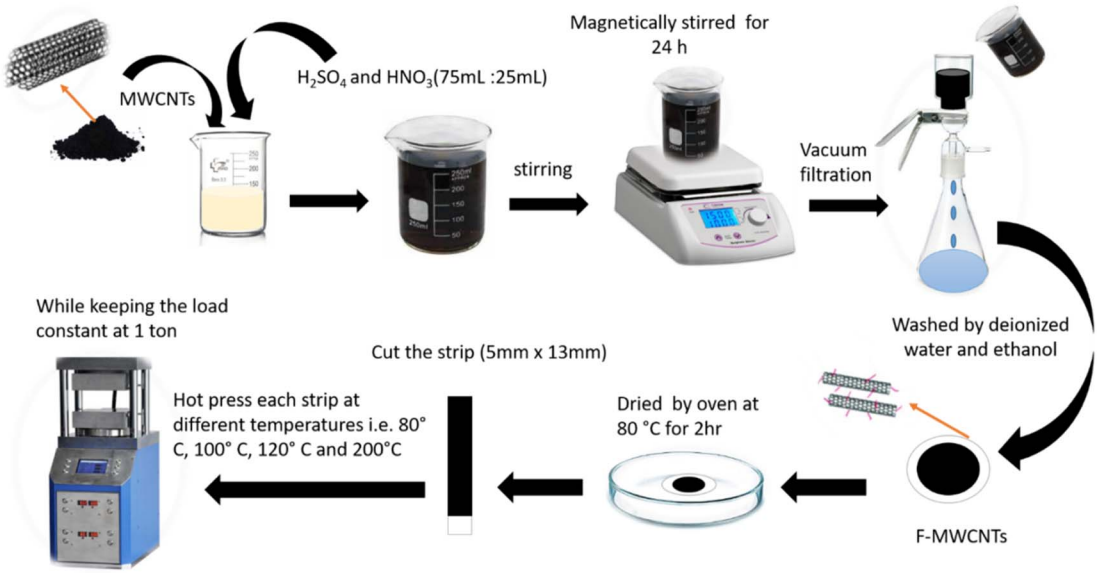

Fig. 1 Experimental sequence involving the functionalization of carbon nanotubes (CNTs) followed by preparation of film through vacuum filtration. The obtained film were cut into segments having dimensions of 5 mm × 13 mm and then subjected to hot-pressing at different temperatures of 80 °C, 100 °C, 120 °C, and 200 °C.

intensity ratio of the D-band to the G-band (D/G). The morphological and elemental studies of all the samples were carried out using scanning electron microscopy (SEM: TESCAN Mira-3) equipped with energy-dispersive X-rays (EDX) detector (Oxford). The electrical conductivity and Seebeck coefficient were measured using Thermoelectric Parameter Test System (NAMICRO-3L) by Joule Yacht, China.

Namicro-3 thermoelectric measurement system is primarily designed for testing bulk thermoelectric materials. However, in the present scenario, CNT's deposited over flexible substrate is kind of thick films having thickness several hundreds of micron. Secondly, these samples were first placed over glass slides to make the samples fitted into the sample holder. As we are aware, the main distinction between the bulk system and the films lies in the contacts making. To address this issue, we've used copper tape, considering that the sample holder is also made up of copper. This approach ensures a reliable connection and allows us to effectively test thin film materials using the Namicro-3 system.

3 Results and discussion

The chemical composition and molecular structure of multi-walled carbon nanotubes (MWCNTs) and functionalized multi-walled carbon nanotubes (F-MWCNTs) are determined by Fourier-transform infrared spectroscopy (FTIR) shown in Fig. 2(a). The technique works by measuring how different molecular bonds absorb infrared light at various frequencies, which correspond to different vibrational modes of the bonds. The phenomenon of electron transfer plays a crucial role in peak shifts of FTIR spectra. Electron transfer can lead to a redistribution of electron density within the molecule. During acid treatment, when functional groups are introduced to the surface of MWCNTs, such as carboxylic acid groups (–COOH), the electron density around the carbon atoms in the nanotube structure is altered. This change in electron density affects the bond strength and the vibrational energy levels of the atoms involved, leading to shifts in the absorption peaks in the FTIR spectrum. The stretching vibration of a bond depends on the bond strength and the masses of the atoms involved. When electron-accepting groups like –COOH are grafted onto MWCNTs, they can pull electron density away from the carbon atoms in the nanotube. This electron withdrawal can increase the effective bond strength of adjacent carbon–carbon bonds, leading to higher vibrational frequencies and thus shifts in the FTIR peaks.

The peak at 1636 cm^{-1} in MWCNTs, shows C=C stretching in aromatic rings, is observed due to the intrinsic electron distribution in the pristine nanotube structure.[69] Upon functionalization, new peaks appear at 1720 cm^{-1} and 1576 cm^{-1} in F-MWCNTs. The 1720 cm^{-1} peak corresponds to the stretching vibrations of the carbonyl group (C=O) in carboxylic acids, indicating the presence of –COOH groups.[70] The 1576 cm^{-1} peak represents stretching vibrations associated with carboxylate anions (COO–), suggesting deprotonation of carboxylic acid groups.[71] The appearance of new peaks in the FTIR spectrum of F-MWCNTs directly correlates with the introduction of specific functional groups. The shifts to higher or lower wavenumbers are indicative of different electronic environments and bond strengths. The peak at 1560 cm^{-1} in F-MWCNTs shows the carboxylate anion stretch mode, verifying the presence of carboxylate groups.[72] This peak indicates the successful grafting of carboxyl groups onto the MWCNT surface, altering the electron distribution and causing a peak shift compared to the pristine MWCNT spectrum.[73]

Similar results have been documented in the literature,[74,75] where functionalization of carbon nanotubes with various

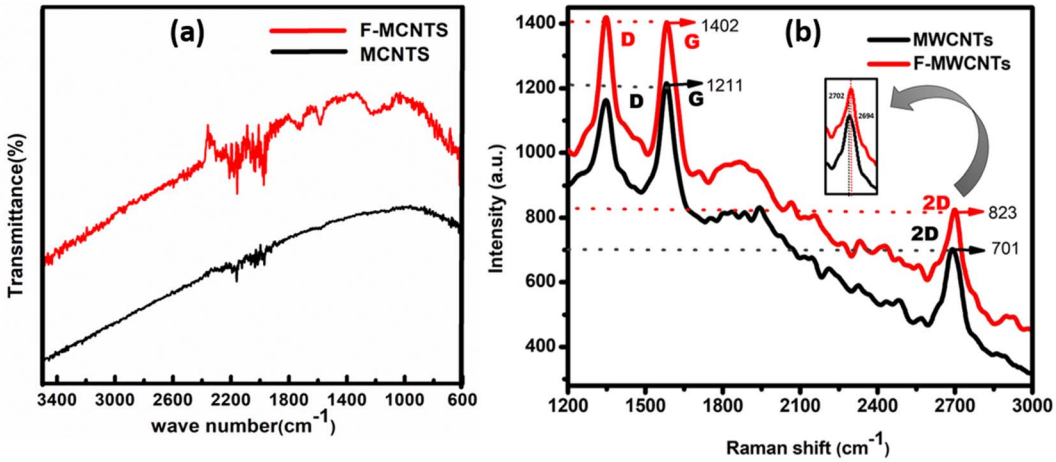

Fig. 2 Fourier transform infrared (FTIR) spectroscopy (a) and Raman spectroscopy (b) data of multi-walled carbon nanotubes (MWCNTs) and functionalized multi-walled carbon nanotubes (F-MWCNTs).

groups leads to distinct shifts in FTIR peaks. These shifts are a result of changes in the electronic structure and bonding characteristics due to electron transfer and redistribution upon functionalization. Studies have consistently shown that grafting functional groups onto MWCNTs results in characteristic FTIR peaks that are different from those of pristine MWCNTs, confirming the chemical modifications. Understanding these shifts allows researchers to confirm the successful functionalization of MWCNTs and to characterize the new chemical environments created by these modifications.

To check the purity and structural characteristics of MWCNTs and F-MWCNTs powders we performed Raman spectroscopy analysis, as presented in Fig. 2(b). By examining the specific vibrational modes of carbon atoms within the nanotube structure, Raman spectroscopy provides insights into the degree of order, presence of defects, and electronic interactions within the material. This phenomenon has a significant impact on the observed peak shifts in Raman spectra related to electron transfer.

Functionalization often involves introducing chemical groups or treating the nanotubes with substances such as ammonia (NH_3). This can result in electron transfer between the functional groups or molecules and the carbon nanotube structure. The D band in Raman spectra, observed at approximately 1341 cm^{-1}, is associated with sp^3 hybridization and indicates the presence of defects or impurities in the carbon nanotube structure.[76] When electron transfer occurs, the altered electron density around defect sites can modify the vibrational characteristics of these regions, potentially causing shifts in the D band position or intensity. In MWCNTs D band appears at around 1347 cm^{-1} and for F-MWCNTs the D band appears at around 1349 cm^{-1}, indicating the presence of defects or disorder within the nanotube structure.

The G band, which appears between 1550 cm^{-1} and 1600 cm^{-1}, is linked to sp^2 hybridization and reflects the degree of order within the graphene structure of the nanotubes.[77] Electron transfer can influence the electron cloud around sp^2 hybridized carbon atoms, leading to changes in bond strength and vibrational frequency. Shifts or changes in intensity can indicate changes in graphitic structure due to functionalization or defects. The G band appears at approximately 1577 cm^{-1} in MWCNTs and shifts slightly to 1571 cm^{-1} in F-MWCNTs. This shift indicates changes in the electronic environment and structural order due to functionalization and electron transfer.[78] Extensive research has revealed similar G-band shifts when carbon nanotubes are functionalized with various amine groups and other electron-donating species.[79–82] These studies provide a consistent theoretical framework for understanding the electron transfer mechanisms involved.

The 2D band, also known as the G′ band, observed at approximately 2700 cm^{-1}, provides information about the electronic structure and stacking order of the graphene layers.[83,84] Changes in the electron density resulting from electron transfer can affect the interlayer interactions and the overall electronic structure, leading to shifts in the 2D band position. The 2D band shifts from around 2688 cm^{-1} in MWCNTs to approximately 2701 cm^{-1} in F-MWCNTs, reflecting such electronic modifications.[85]

During functionalization, such as acid treatment involving ammonia, NH_3 molecules can interact with the carbon nanotube structure. Ammonia has the ability to either donate or accept electrons. In this case, it donates electrons to the nanotube structure. This electron donation can influence the vibrational modes of the carbon atoms, as observed in the Raman spectra. The interaction between NH_3 and the nanotubes can introduce new defects or enhance existing ones, leading to changes in the G and D band intensity and position. The functionalization process likely introduced electron-accepting groups (such as carboxyl or hydroxyl) onto the MWCNT surface. These groups withdraw electrons from the nanotube structure, leading to the observed G-band shift in F-MWCNTs, where the electron-accepting effects surpass NH_3's donor effect.

The increase in the I_D/I_G ratio from 0.96 in unmodified MWCNTs to 1.01 in F-MWCNTs indicates a higher defect density in F-MWCNTs, endorsing the influence of electron transfer and the introduction of structural disruptions due to

functionalization.[86–88] The comparative analysis of the D and G peaks in Raman spectra helps in assessing the purity and degree of functionalization of the nanotubes. The increase in the D/G ratio for F-MWCNTs compared to MWCNTs suggests a decline in graphitic quality and the introduction of defects due to electron transfer and functional group attachment. These changes are crucial for understanding how the material's properties, such as electrical conductivity and mechanical strength, are affected by functionalization.

Functionalization of MWCNTs with the help of H_2SO_4 and HNO_3 led to oxidation and increased graphitization, promoting a transition from multi-layer to single-layer structures. This transformation enhances electron mobility and reduces charge scattering, improving the electrical and thermoelectric properties of the flexible films. The graphitization observed in our samples suggests that multi-layer structures are transitioning into more conjugated, single-layer configurations. The intensity ratios calculated from the 2D band to the G-band further support the presence of single-layer configurations.

The I_{2D}/I_G ratio is a key indicator in Raman spectroscopy for assessing the quality and layer count in graphene materials. Functionalization of MWCNTs increases the I_{2D}/I_G ratio by reducing defects and improving graphitic structure, enhancing sp^2 hybridization and structural order. This process passivates surface defects, reduces Raman signal scattering, and improves the material's electronic properties, leading to better quality for applications requiring high conductivity and strength.[84,89–91]

The I_{2D}/I_G ratios we calculated for the MC graph show a value of approximately 0.57 indicating a multi-layer structure. In contrast, the graph of FC sample yields an I_{2D}/I_G ratio of approximately 0.622. This value supports our hypothesis that the functionalization process has significantly altered the structural properties, leading to enhanced electronic characteristics.

Scanning electronic microscope (SEM) images of the as-deposited functionalized multi-walled carbon nanotubes (F-MWCNTs) film and functionalized multi-walled carbon nanotubes (F-MWCNTs) film subjected to hot-pressing at 120 °C are shown in Fig. 3(a) and (b), respectively. As per reported data, during the functionalization process, COOH and OH groups were formed on the sidewalls and caps of the MWCNTs.[92] These functional groups can interact chemically or physically with other functional groups in the CNTs to increase the dispersion and create a strong interfacial adhesion.

A study demonstrated that oxidative treatment of multi-walled carbon nanotubes (MWCNTs) can reduce the length of the nanotubes, leading to the formation of smaller-sized aggregates.[92] Agglomerates of CNTs with some porosity can be seen clearly before hot-pressing as shown in Fig. 3(a). Hot-pressing is a technique that involves applying high pressure and temperature to a material to densify it. This process can effectively reduce porosity in materials like MWCNTs by filling in the gaps between the nanotubes and the surrounding matrix. In the study on buck papers, hot-pressing at 70 °C greatly reduced porosity, which resulted in improved thermal and electrical conductivity.[61] This densification facilitated the formation of integrated crystal boundaries in the PVA,

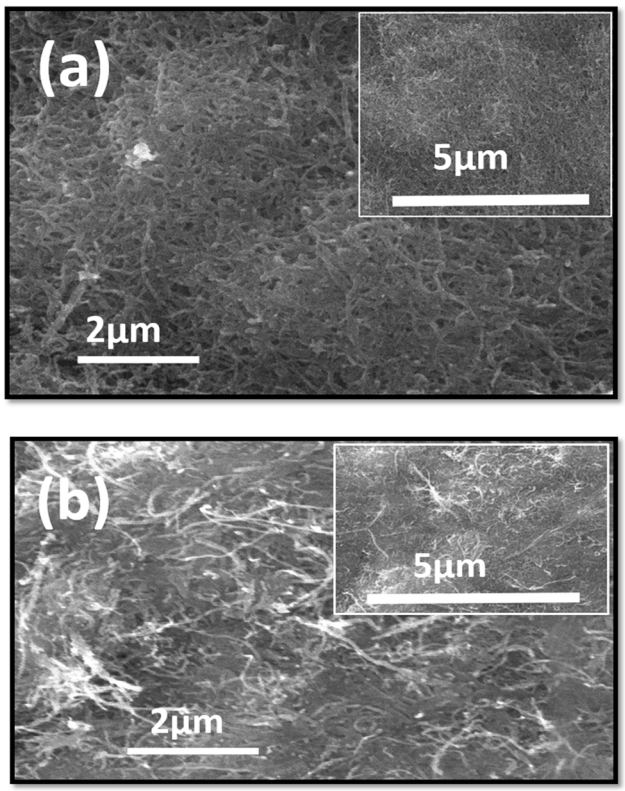

Fig. 3 Scanning electronic microscope (SEM) images of the as-deposited functionalized multi-walled carbon nanotubes (F-MWCNTs) film (a) and functionalized multi-walled carbon nanotubes (F-MWCNTs) film subjected to hot-pressing at 120 °C (b).

increasing the phonon mean free path and enhancing thermal conductivity. Hot-pressing can also enhance the alignment of MWCNTs by applying mechanical stress and pressure. This process can align the nanotubes along the direction of the applied force, leading to improved mechanical and electrical properties. As in the above mentioned study on MWCNT/PVA buck papers, hot-pressing at 70 °C (ref. 61) improved the alignment of MWCNTs, resulting in enhanced electrical conductivity from 463.5 S m^{-1} to 714.3 S m^{-1}.[93] However, another study demonstrated that hot-pressing can align MWCNTs in alumina composites, leading to improved mechanical and tribological properties. The reduction in entanglement of MWCNTs during acid treatment followed by hot-pressing is due to several mechanisms: shear force[94] aligns them along the force direction, mechanical stretch elongates them in the force direction, and high pressure and temperature enhance interfacial bonding, improving alignment and reduces the entanglement.[95] After hot-pressing, the porosity of MWCNTs is reduced and CNT's entanglement is reduced, which enhances the interconnection of CNTs, as illustrated in Fig. 3(b), which is in agreement with the previously reported data as well.[67,96]

The temperature depending electrical conductivity of all the series of samples is shown in Fig. 4(a). The aggregation is significantly reduced by chemical functionalization, thereby improving electrical conductivity of as-deposited MWCNTs.[97] The hot-pressing has results into a further increase in the

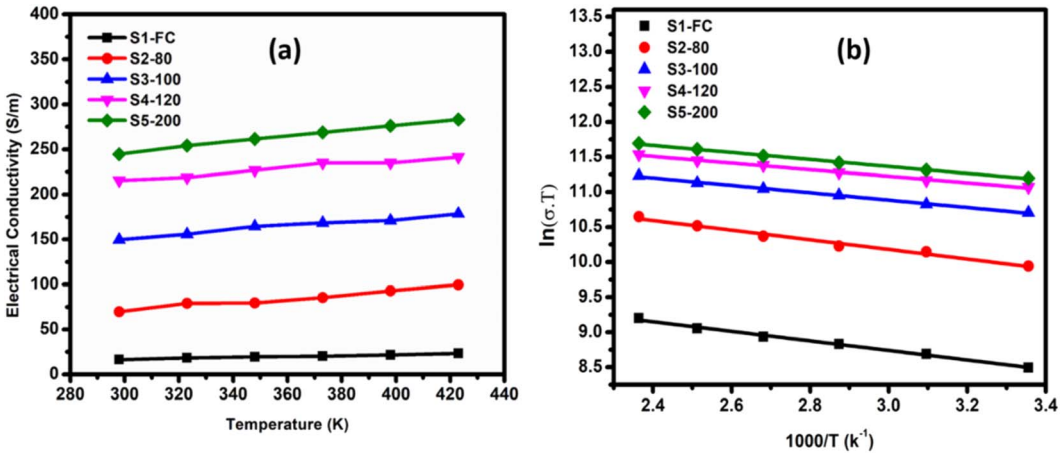

Fig. 4 Temperature dependent electrical conductivity (a) and activation energy (b) of as-deposited functionalized multi-walled carbon nanotubes (F-MWCNTs) film and functionalized multi-walled carbon nanotubes (F-MWCNTs) films subject to hot-pressing at temperatures 80 °C, 100 °C, 120 °C, and 200 °C.

electrical conductivity of all the series. It can also be noted that increase in hot-press temperature resulted in the increased electrical conductivity, which is in good agreement with the literature.[98] The highest electrical conductivity value of 283 S m^{-1} has been achieved for S5-200 at 423k, which is even greater than the already reported value for CNTs' film.[99–101] From the insights provided by previous studies, we can say that hot press encourages closer contacts between the MWCNTs, which results in improved tube-to-tube contacts.[59] The total number of contact points increase under heat and pressure and the tubes get closer together which results in increasing carrier mobility. This reduction in entanglement and porosity promotes effective charge transport throughout the nanotubes, increasing the electrical conductivity.[102]

Fig. 4(b) shows a logarithmic dependence of electrical conductivity *vs.* inverse of temperature ($1/T$), which helps to explain the temperature-dependent behavior of electrical conductivity to allow the determination activation energy and provides insights into the material's transport properties. It is an important aspect to optimize the thermoelectric performance. Every hot-pressed film had linear characteristics, which represent the films' semiconductor behavior throughout the temperature region. The activation energy (E_g) of carriers in the films can determined by the expression as given in the eqn (1).[103]

$$\sigma = \sigma_0 \exp\left(-\frac{E_g}{K_B T}\right) \quad (1)$$

where σ_0 is the temperature-independent part of conductivity, (K_B) is the Boltzmann constant, and T is the absolute temperature. The calculated E_g values for all the samples S1-FC, S2-80, S3-100, S4-120 and S5-200 are 58.84 meV, 59.36 meV, 45.27 meV, 42.95 meV and 42.95 meV, respectively. A significatn decrease in E_g has been observed after hot-pressing of the films which infers about improved conducting channels in the samples.

The Seebeck coefficient of MWCNT films can range from a few microvolts to thousands of microvolts per kelvin, depending on the specific composition and processing conditions. Strategies like doping, functionalization, and hybrid structures have been effective in enhancing the thermoelectric performance of MWCNT films. One study shows that nitrogen-doped MWCNTs (N-MWCNTs) exhibit negative Seebeck coefficients in epoxy composites.[60] In another study, the Seebeck coefficient of $Bi_{0.4}Sb_{1.6}Te_3$-MWCNTs reaches its maximum value at 160 K and decreases to 409 μV K^{-1} at 300 K.[62] Furthermore, research shows that hot-pressing MWCNT/PVA buck papers at 70 °C significantly increases the Seebeck coefficient from 463.5 S m^{-1} to 714.3 S m^{-1}.[61]

The anomalous behavior of the Seebeck coefficient in the temperature range of 350–390 K is unlikely due to a phase transformation. MWCNTs, being carbon-based nanomaterials, have a stable structure over a broad temperature range, and functionalization typically introduces chemical groups and defects without causing phase changes. The moderate temperature range of 350–390 K is not sufficient to induce phase transformations in MWCNTs, which usually occur at much higher temperatures (above 2000 K).

At 350 K (77 °C), the temperature is relatively low and is unlikely to significantly affect the strong carbon–carbon bonds in the CNTs themselves. However, the functional groups attached to the CNTs, such as carboxyl (–COOH) and hydroxyl (–OH) groups, might still experience changes even at this lower temperature due to weaker bonding to the CNT surface compared to the intrinsic CNT structure. Increased thermal energy can cause vibrations that may weaken the interactions between CNTs and attached functional groups, leading to partial detachment or reorientation. Even if the functional groups don't completely detach, they may reorient on the CNT surface, altering the electronic and chemical properties. Additionally, subtle changes at the interface between the CNTs and any matrix material can affect the overall material properties. Therefore, while the core structure of the CNTs remains intact, the functional groups can still undergo changes that impact the material's behavior.

At 200 °C, functional groups like –COOH and –OH might degrade or detach from the CNT surface, altering electronic properties. Hot pressing at this temperature can cause

structural reorganization in the CNT network, leading to densification and reorientation, which impacts thermal and electrical pathways. The process also enhances interactions between CNTs and the matrix material, potentially creating new interfacial states that influence conductivity and thermoelectric behavior. Additionally, residual stresses introduced during hot pressing affect the material's properties, contributing to the observed negative Seebeck for S5-200.

The Seebeck coefficient trends of S1-FC, S2-80, S3-100, S4-120 and S5-200 presented in Fig. 5(a) exhibit p-type semiconductor behavior because NH_3 transfer electrons to the underlying nanotube structure during acid treatment.[104] The transferred electrons will recombine with holes, thereby decreasing the charge carrier concentration.[105] The sample S4-120 shows the highest Seebeck coefficient value of 116 $\mu V\ K^{-1}$ at 398 K, which is relatively high compared to other studies on MWCNT films. The Seebeck coefficient of all samples exhibits a noticeable change in trend within the temperature range of 360 K to 380 K which may be associated to the partial detachment or reorientation of functional groups. Secondly, the Seebeck coefficient measurement method has an intrinsic error of about 8–10% due to simultaneous heating by the heating filament to maintain a temperature gradient between two ends of the samples along with heating provided by the furnace chamber to keep the entire environment at an elevated temperature.

As we know that the bulk samples generally exhibit an inherent measurement error, which is often around 10% under optimal conditions. This level of error can be attributed to factors such as the material's homogeneity and slight variances in experimental conditions. Given that our study deals with thin films, these films tend to be even more sensitive to such variations, leading to a natural increase in measurement error. Thin film samples, unlike bulk materials, are more susceptible to interface effects, thermal fluctuations, and substrate interactions, which can amplify inconsistencies in the Seebeck coefficient readings. We have attempted to reproduce the measurements as accurately as possible within these constraints. However, we are unable to provide multiple measurements across different samples to reduce variability statistically because of limited by sample availability.

The power factor ($PF = \sigma S^2$) is directly proportional to the product of the electrical conductivity (σ) and the square of the Seebeck coefficient (S). From this, it can be inferred that for better thermoelectric PF, a material should have larger electrical conductivity and Seebeck coefficients. We achieved the highest power factor (PF) value of approximately 3.17 $\mu W\ m^{-1}\ K^{-2}$ at 398 K for sample S4-120, attributed to its higher electrical conductivity (σ) and Seebeck coefficient (S) values, shown in Fig. 5(b). Previously, the maximum power factor reported for MWCNT films after functionalization and hot-pressing was around 0.51 $\mu W\ m^{-1}\ K^{-2}$, observed with PPy/MWCNTs-SH, which represents an eightfold enhancement compared to pure PPy.[106]

Electronic thermal conductivity (k_e) in thermoelectrics refers to a material's capacity to transfer heat *via* charge carriers (holes/electrons) motion. It affects thermoelectric system optimization and the effectiveness of converting heat to electrical energy. Effective heat transfer and superior electrical conductivity are favored for better thermoelectric performance, with high electronic thermal conductivity being the key. It can be calculated by eqn (2):

$$K_e = L_o \sigma T \quad (2)$$

where k_e is the electronic thermal conductivity, L_o is the Lorentz number and T is the working temperature. Fig. 6, Shows k_e for all the series of samples with an increasing trend with temperature. The interaction of variables like higher electrical conductivity and potential change in the Seebeck coefficient can be used to explain this behavior. The elevated electrical conductivity results from increased charge carrier mobility (electrons) within films film at higher temperatures. This larger ability of the material to conduct heat through electron/holes movement is indicated by a better electronic thermal conductivity, which is influenced by the improved electrical conductivity.

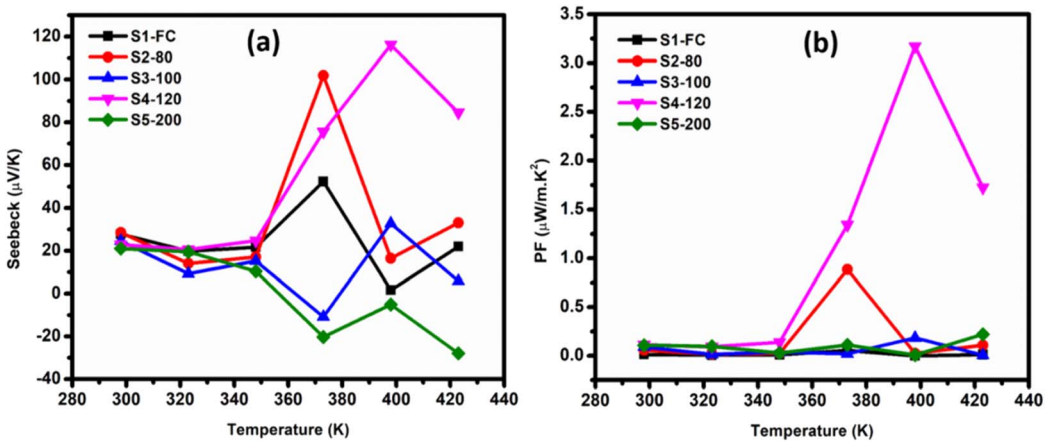

Fig. 5 Temperature dependent Seebeck coefficient (a) and thermoelectric power factor (PF) (b) of as-deposited functionalized multi-walled carbon nanotubes (F-MWCNTs) film and functionalized multi-walled carbon nanotubes (F-MWCNTs) films subject to hot-pressing at temperatures 80 °C, 100 °C, 120 °C, and 200 °C.

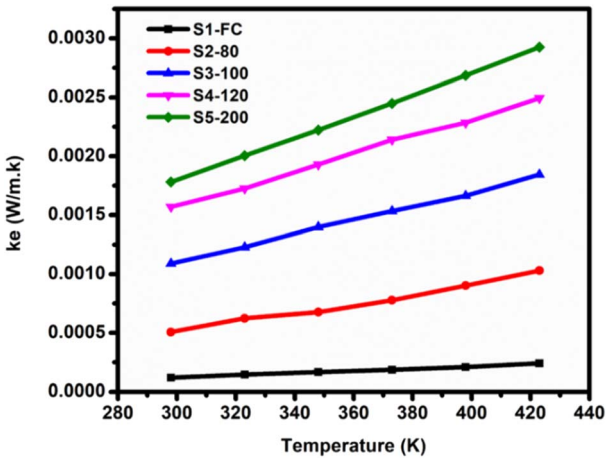

Fig. 6 Temperature dependent electronic thermal conductivity (k_e) of as-deposited functionalized multi-walled carbon nanotubes (F-MWCNTs) film and functionalized multi-walled carbon nanotubes (F-MWCNTs) films subject to hot-pressing at temperatures 80 °C, 100 °C, 120 °C, and 200 °C.

4 Conclusion

We successfully functionalized multi-walled carbon nanotubes (MWCNTs) through conventional acid treatment followed by their deposition over flexible substrates through a facile route of vacuum filtration. The as-deposited functionalized multi-walled carbon nanotubes (F-MWCNTs) films were hot-pressed at various temperatures of 80 °C, 100 °C, 120 °C, and 200 °C, under a constant uniaxial pressure of 1 ton for 60 s. Our results show that by increasing the hot-pressing temperature, the electrical conductivity increases. The S5-200 sample hot-pressed at 200 °C, exhibits the highest electrical conductivity of 283 S m^{-1} at 423 K. On the other hand, the S4-120 sample hot-pressed at 120 °C, exhibits the electrical conductivity of 241 S m^{-1} at 400 K along with the highest Seebeck coefficient value of 115 μV K^{-1} which results in the highest power factor approx. 3.17 μW m^{-1} K^{-2} at 398 K. Our results emphasize the significance of facile vacuum filtration route coupled with hot-pressing in regulating the thermoelectric properties of flexible CNTs films.

Data availability

Graphical data presented in the manuscript and numerical data will be available on request. All details are mentioned in the manuscript.

Conflicts of interest

All the authors declare that there have no conflicts of interest.

Acknowledgements

All the authors are thankful to the Higher Education Commission (HEC) of Pakistan for financial support through the 8096/NRPU/R&D/HEC/2017 project.

References

1 T. Bachagha and J.-J. Suñol, *Metals*, 2023, **13**, 111.
2 H. Mamur, Ö. F. Dilmaç, J. Begum and M. R. A. Bhuiyan, *Clean. Mater.*, 2021, **2**, 100030.
3 H. Scherrer, D. Rowe, T. Kajikawa, K. Matsubara, J.-P. Issi, H. J. Goldsmid, C. M. Bhandari, A. T. Burkov, V. K. Zaitsev and M. I. Fedorov, *Thermoelectrics Handbook: Macro to Nano*, 2018, DOI: 10.1201/9781420038903.
4 C. B. Vining, *Nature*, 2001, **413**, 577–578.
5 H. J. Goldsmid, *Introduction to Thermoelectricity*, Springer, 2016, vol. 121.
6 W. Liu, H. S. Kim, Q. Jie and Z. Ren, *Scr. Mater.*, 2016, **111**, 3–9.
7 W. Liu, H. S. Kim, S. Chen, Q. Jie, B. Lv, M. Yao, Z. Ren, C. P. Opeil, S. Wilson and C.-W. Chu, *Proc. Natl. Acad. Sci. U. S. A.*, 2015, **112**, 3269–3274.
8 G. Ren, J. Lan, C. Zeng, Y. Liu, B. Zhan, S. Butt, Y.-H. Lin and C.-W. Nan, *JOM*, 2015, **67**, 211–221.
9 Y. Shi, C. Sturm and H. Kleinke, *J. Solid State Chem.*, 2019, **270**, 273–279.
10 A. Maignan, E. Guilmeau, F. Gascoin, Y. Bréard and V. Hardy, *Sci. Technol. Adv. Mater.*, 2012, **13**, 053003.
11 A. I. Romanenko, G. E. Chebanova, T. Chen, W. Su and H. Wang, *J. Phys. D: Appl. Phys.*, 2021, **55**, 143001.
12 S. Butt, W. Xu, M. U. Farooq, G. K. Ren, F. Mohmed, Y. Lin and C. Nan, *J. Am. Ceram. Soc.*, 2015, **98**, 1230–1235.
13 M. U. Iqbal, S. Butt, M. U. Farooq, S. Hussain, S. Irfan, N. Ali, M. A. Basit, M. A. Akram, M. Yasir and A. Hassan, *Phys. Rev. B*, 2023, **654**, 414738.
14 Y. Liu, Y. Zheng, B. Zhan, K. Chen, S. Butt, B. Zhang and Y. Lin, *J. Eur. Ceram. Soc.*, 2015, **35**, 845–849.
15 S. Butt, Y. Ren, M. U. Farooq, B. Zhan, R. U. R. Sagar, Y. Lin and C.-W. Nan, *Energy Convers. Manag.*, 2014, **83**, 35–41.
16 S. Butt, W. Xu, W. Q. He, Q. Tan, G. K. Ren, Y. Lin and C.-W. Nan, *J. Mater. Chem. A*, 2014, **2**, 19479–19487.
17 M. Rull-Bravo, A. Moure, J. F. Fernández and M. Martín-González, *RSC Adv.*, 2015, **5**, 41653–41667.
18 G. Rogl and P. Rogl, *Curr. Opin. Green Sustain. Chem.*, 2017, **4**, 50–57.
19 C. Uher, in *Semiconductors and Semimetals*, Elsevier, 2001, vol. 69, pp. 139–253.
20 X. Li, P. Yang, Y. Wang, Z. Zhang, D. Qin, W. Xue, C. Chen, Y. Huang, X. Xie, X. Wang, M. Yang, C. Wang, F. Cao, J. Sui, X. Liu and Q. Zhang, *Research*, 2020, **2020**, 4630948.
21 H. Zhu, J. Mao, Y. Li, J. Sun, Y. Wang, Q. Zhu, G. Li, Q. Song, J. Zhou and Y. Fu, *Nat. Commun.*, 2019, **10**, 270.
22 B. Rani, A. F. Wani, U. B. Sharopov, L. Patra, J. Singh, A. M. Ali, A. F. Abd El-Rehim, S. A. Khandy, S. Dhiman and K. Kaur, *Molecules*, 2022, **27**, 6567.
23 K. Kishimoto and K. Akai, *J. Solid State Chem.*, 2023, **324**, 124122.
24 J.-A. Dolyniuk, B. Owens-Baird, J. Wang, J. V. Zaikina and K. Kovnir, *Mater. Sci. Eng., R*, 2016, **108**, 1–46.
25 R. Freer, D. Ekren, T. Ghosh, K. Biswas, P. Qiu, S. Wan, L. Chen, S. Han, C. Fu, T. Zhu, A. K. M. Ashiquzzaman

Shawon, A. Zevalkink, K. Imasato, G. J. Snyder, M. Ozen, K. Saglik, U. Aydemir, R. Cardoso-Gil, E. Svanidze, R. Funahashi, A. V. Powell, S. Mukherjee, S. Tippireddy, P. Vaqueiro, F. Gascoin, T. Kyratsi, P. Sauerschnig and T. Mori, *J. Phys.: Energy*, 2022, **4**, 022002.
26 M. W. Akram, S. Butt, M. Saadullah, M. Irfan, M. A. Basit and M. A. Akram, *J. Mater. Sci.:Mater. Electron.*, 2024, **35**, 272.
27 Z. Afzal, S. Butt, M. Rizwan, S. U. Rehman, S. Sajjad, Z. Usman and G. M. Murtaza, *Next Mater.*, 2025, **7**, 100383.
28 T. Ahmed, T. Farooq, K. Ahmed, M. A. U. Rehman, M. Yasir, S. Butt and M. A. Basit, *Colloids Surf., A*, 2024, **691**, 133850.
29 D. Jung, M. Han and G. S. Lee, *J. Vac. Sci. Technol. B.*, 2014, **32**, DOI: 10.1116/1.4883050.
30 A. Abdelhalim, A. Abdellah, G. Scarpa and P. Lugli, *Carbon*, 2013, **61**, 72–79.
31 L. Hu, D. S. Hecht and G. Grüner, *Chem. Rev.*, 2010, **110**, 5790–5844.
32 J. A. Misewich, R. Martel, P. Avouris, J. C. Tsang, S. Heinze and J. Tersoff, *Science*, 2003, **300**, 783–786.
33 C. H. Lau, R. Cervini, S. R. Clarke, M. G. Markovic, J. G. Matisons, S. C. Hawkins, C. P. Huynh and G. P. Simon, *J. Nanopart. Res.*, 2008, **10**, 77–88.
34 K. Shehzad, Z.-M. Dang, M. N. Ahmad, R. U. R. Sagar, S. Butt, M. U. Farooq and T.-B. Wang, *Carbon*, 2013, **54**, 105–112.
35 J. Espadas-Escalante, F. Avilés, P. Gonzalez-Chi and A. Oliva, *J. Cell. Plast.*, 2017, **53**, 215–230.
36 A. V. Radhamani, H. C. Lau and S. Ramakrishna, *Composites, Part A*, 2018, **114**, 170–187.
37 M. Bhattacharya, *Materials*, 2016, **9**, 262.
38 R. Rauti, M. Musto, S. Bosi, M. Prato and L. Ballerini, *Carbon*, 2019, **143**, 430–446.
39 M. Zhang and J. Li, *Mater. Today*, 2009, **12**, 12–18.
40 S. Dumonteil, A. Demortier, S. Detriche, C. Raes, A. Fonseca, M. Rühle and J. B. Nagy, *J. Nanosci. Nanotechnol.*, 2006, **6**, 1315–1318.
41 K. Yang, Z. Yi, Q. Jing, R. Yue, W. Jiang and D. Lin, *Chin. Sci. Bull.*, 2013, **58**, 2082–2090.
42 A. Hirsch and O. Vostrowsky, in *Functional Molecular Nanostructures*, ed. A. D. Schlüter, Springer Berlin Heidelberg, Berlin, Heidelberg, 2005, vol. 245, pp. 193–237.
43 V. Datsyuk, M. Kalyva, K. Papagelis, J. Parthenios, D. Tasis, A. Siokou, I. Kallitsis and C. Galiotis, *Carbon*, 2008, **46**, 833–840.
44 K. A. Worsley, I. Kalinina, E. Bekyarova and R. C. Haddon, *J. Am. Chem. Soc.*, 2009, **131**, 18153–18158.
45 S.-H. Chung, D. H. Kim, H. Kim, H. Kim and S. W. Jeong, *Mater. Today Commun.*, 2020, **23**, 100867.
46 K. Nishimura, T. Ushiyama, N. X. Viet, M. Inaba, S. Kishimoto and Y. Ohno, *Electrochim. Acta*, 2019, **295**, 157–163.
47 B. Xie, G. Xu, Y. Jia, L. Gu, Q. Wang, N. Mushtaq, B. Cheng and Y. Hu, *J. Membr. Sci.*, 2021, **625**, 118978.
48 S.-C. Her and W.-C. Hsu, *Sensors*, 2020, **20**, 3067.
49 S. Roy, V. Jain, R. Bajpai, P. Ghosh, A. S. Pente, B. P. Singh and D. S. Misra, *J. Phys. Chem. C*, 2012, **116**, 19025–19031.
50 H. Chen, M. Chen, J. Di, G. Xu, H. Li and Q. Li, *J. Phys. Chem. C*, 2012, **116**, 3903–3909.
51 S. S. Isa, M. M. Ramli, M. F. Jamlos, N. A. M. Hambali, M. M. Isa, S. R. Kasjoo, N. Ahmad, N. I. M. Nor and N. Khalid, in *AIP Conference Proceedings*, AIP Publishing, 2017, vol. 1808.
52 M. I. Shahzad, M. Giorcelli, L. Ventola, D. Perrone, N. Shahzad, E. Chiavazzo, P. Asinari, M. Cocuzza and A. Tagliaferro, *Heat Transfer Eng.*, 2016, **37**, 783–790.
53 A. Nag, M. E. E. Alahi, S. C. Mukhopadhyay and Z. Liu, *Sensors*, 2021, **21**, 1261.
54 M. Al-Bahrani, H. S. Majdi, A. M. Abed and A. Cree, *Int. J. Energy Res.*, 2022, **46**, 7519–7528.
55 J. J. Kuchle and N. D. Love, *Measurement*, 2014, **47**, 26–32.
56 A. Sathishkumar and M. Cheralathan, *Environ. Sci. Pollut. Res.*, 2022, **29**, 38493–38504.
57 M. Nawwar, R. P. Sahu, I. K. Puri and I. Zhitomirsky, *Front. Energy Res.*, 2020, **8**, 46.
58 B. J. Landi, M. J. Ganter, C. D. Cress, R. A. DiLeo and R. P. Raffaelle, *Energy Environ. Sci.*, 2009, **2**, 638–654.
59 W. Lee, Y. H. Kang, J. Y. Lee, K.-S. Jang and S. Y. Cho, *Mater. Today Commun.*, 2017, **10**, 41–45.
60 B. Kumanek, G. Stando, P. S. Wróbel and D. Janas, *Materials*, 2019, **12**, 3567.
61 L. Cao, Y. Liu, J. Wang, Y. Pan, Y. Zhang, N. Wang and J. Chen, *Nanomaterials*, 2020, **10**, 2503.
62 S. C. Tseng, C.-A. Wang, H. S. Chu and H.-Y. Tsai, *J. Mater. Sci.*, 2022, **57**, 19396–19404.
63 J.-F. Brun, C. Binet, J.-F. Tahon, A. Addad, P. Tranchard and S. Barrau, *Synth. Met.*, 2020, **269**, 116525.
64 N. Chen, C. Ren, L. Sun, H. Xue, H. Yang, X. An, X. Yang, J. Zhang and P. Che, *CrystEngComm*, 2022, **24**, 260–268.
65 Y. Bai, X. Li, T. Ouyang, W. Wang, Y. Yan, X. Jiang, X. Wang, Z. Wang, X. Cai and J. Cai, *Carbon*, 2023, **212**, 118158.
66 J. Y. Kim and J. C. Grossman, *Nano Lett.*, 2015, **15**, 2830–2835.
67 K. Jirakittidul, N. Vittayakorn, R. Manrean, N. Pornteeranawapat and S. Neamyooyong, *Mater. Res. Express*, 2019, **6**, 115003.
68 L. Y. Jun, N. M. Mubarak, L. S. Yon, C. H. Bing, M. Khalid and E. C. Abdullah, *J. Environ. Chem. Eng.*, 2018, **6**, 5889–5896.
69 H. Peng, L. B. Alemany, J. L. Margrave and V. N. Khabashesku, *J. Am. Chem. Soc.*, 2003, **125**, 15174–15182.
70 F. Du, K. Wu, Y. Yang, L. Liu, T. Gan and X. Xie, *Nanotechnology*, 2008, **19**, 085716.
71 S. Sahebian, S. M. Zebarjad, J. Vahdati Khaki and A. Lazzeri, *J. Nanostructure Chem.*, 2015, **5**, 287–293.
72 S. Chen, Z. Chen, Y. Ou, J. Lyu, J. Li, X. Liu and Y. Liu, *Composites, Part A*, 2024, **177**, 107911.
73 M. A. Atieh, O. Y. Bakather, B. Al-Tawbini, A. A. Bukhari, F. A. Abuilaiwi and M. B. Fettouhi, *Bioinorg. Chem. Appl.*, 2010, **2010**, 603978.
74 S. Hussain, P. Jha, A. Chouksey, R. Raman, S. S. Islam, T. Islam and P. K. Choudhary, *J. Mod. Phys.*, 2011, **2**, 538.

75 C. A. Dyke and J. M. Tour, *J. Phys. Chem. A*, 2004, **108**, 11151–11159.
76 F. Pourfayaz, Y. Mortazavi, A. Khodadadi, S. H. Jafari, S. Boroun and M. V. Naseh, *Appl. Surf. Sci.*, 2014, **295**, 66–70.
77 H. Requardt, A. Braun, P. Steinberg, S. Hampel and T. Hansen, *Toxicol. In Vitro*, 2019, **60**, 12–18.
78 Y. Ouyang, L. M. Cong, L. Chen, Q. X. Liu and Y. Fang, *Phys. E*, 2008, **40**, 2386–2389.
79 P. Puech, E. Flahaut, A. Bassil, T. Juffmann, F. Beuneu and W. Bacsa, *J. Raman Spectrosc.*, 2007, **38**, 714–720.
80 T. Torres, *Angew. Chem., Int. Ed.*, 2011, **50**, 1473–1474.
81 N. S. N. Sa'aya, S. Z. N. Demon, N. Abdullah, A. Shatar, V. F. K. Ernest and N. A. Halim, *Sens. Mater.*, 2019, **31**, 2997–3006.
82 D. Rogala-Wielgus, B. Majkowska-Marzec, A. Zieliński, K. Roszek and M. Liszewska, *RSC Adv.*, 2023, **13**, 30108–30117.
83 B. Tang, H. Guoxin and H. Gao, *Appl. Spectrosc. Rev.*, 2010, **45**, 369–407.
84 I. Childres, L. A. Jauregui, W. Park, H. Cao and Y. P. Chen, *New Dev. Photon Mater. Res.*, 2013, **1**, 1–20.
85 M. S. Dresselhaus, A. Jorio and R. Saito, *Annu. Rev. Condens. Matter Phys.*, 2010, **1**, 89–108.
86 J. H. Lehman, M. Terrones, E. Mansfield, K. E. Hurst and V. Meunier, *Carbon*, 2011, **49**, 2581–2602.
87 A. D. Dobrzańska-Danikiewicz, W. Wolany, D. Łukowiec, K. Jurkiewicz and P. Niedziałkowski, *Nanomater. Nanotechnol.*, 2017, **7**, 184798041770717.
88 N. Gopal, S. Kumar and R. Sahney, *RSC Adv.*, 2021, **11**, 34193–34205.
89 A. Jorio, E. H. M. Ferreira, M. V. O. Moutinho, F. Stavale, C. A. Achete and R. B. Capaz, *Phys. Status Solidi B Basic Res.*, 2010, **247**, 2980–2982.
90 O. Akhavan, E. Ghaderi, E. Hashemi and R. Rahighi, *Nanoscale*, 2014, **6**, 14810–14819.
91 V. Kumar, A. Kumar, D.-J. Lee and S.-S. Park, *Materials*, 2021, **14**, 4590.
92 D. Bikiaris, A. Vassiliou, K. Chrissafis, K. M. Paraskevopoulos, A. Jannakoudakis and A. Docoslis, *Polym. Degrad. Stab.*, 2008, **93**, 952–967.
93 R. I. Rubel, M. H. Ali, M. A. Jafor and M. M. Alam, *AIMS Mater. Sci.*, 2019, **6**, 756–780.
94 H. Zhao, Z. Zhou, H. Dong, L. Zhang, H. Chen and L. Hou, *Sci. Rep.*, 2013, **3**, 3480.
95 K. Ramachandran, V. Boopalan, J. C. Bear and R. Subramani, *J. Mater. Sci.*, 2022, **57**, 3923–3953.
96 T. Mustafa, J. Huang, J. Gao, P. Yan, Y. Liu, K. H. Ruiz, S. Sun, J. Du, Y. Fan and W. Jiang, *J. Eur. Ceram. Soc.*, 2021, **41**, 5541–5547.
97 F. Bordi, C. Cametti, P. Codastefano and P. Tartaglia, *Phys. A: Stat. Mech. Appl.*, 1990, **164**, 663–672.
98 R. Kroon, J. D. Ryan, D. Kiefer, L. Yu, J. Hynynen, E. Olsson and C. Müller, *Adv. Funct. Mater.*, 2017, **27**, 1704183.
99 B. Tserengombo, H. Jeong, E. Dolgor, A. Delgado and S. Kim, *Nanomaterials*, 2021, **11**, 1323.
100 R. Gloukhovski and M. E. Suss, *J. Electrochem. Soc.*, 2020, **167**, 020528.
101 H. Wang, X. Sun, Y. Wang, K. Li, J. Wang, X. Dai, B. Chen, D. Chong, L. Zhang and J. Yan, *Nat. Commun.*, 2023, **14**, 380.
102 P. Gupta, M. Rajput, N. Singla, V. Kumar and D. Lahiri, *Polymer*, 2016, **89**, 119–127.
103 V. D. Das and P. G. Ganesan, *Mater. Chem. Phys.*, 1998, **57**, 57–66.
104 N. Donato, M. Latino and G. Neri, *Carbon Nanotubes:Res. Appl.*, 2011, **14**, 229–242.
105 S. S. Isa, M. M. Ramli, M. Jamlos, N. Hambali, M. M. Isa, S. Kasjoo, N. Ahmad, N. Nor and N. Khalid, *AIP Conf. Proc.*, 2017, **1808**, 020030.
106 Y. B. Cherif, Z. Mekhalif, A. Mekki and Z. B. D. Sayah, *Synth. Met.*, 2022, **291**, 117196.